Supporting Information

Examining the Mechanism of Phosphite Dehydrogenase with Quantum Mechanical/Molecular Mechanical Free Energy Simulations

David R. Stevens and Sharon Hammes-Schiffer*

Department of Chemistry, Yale University, 225 Prospect Street, New Haven, Connecticut 06520

*Corresponding author email: sharon.hammes-schiffer@yale.edu

Table of Contents

Computational Details

All calculations were based on the structure corresponding to the thermostable PTDH with sulfite as the substrate mimic (PDB ID: 4E5K).[1] Among the four chains available within the PDB, chain B was selected because it has the greatest number of active site crystallographic waters, namely three crystallographic waters within 5 Å of the sulfite (HSO_3^{2-}) substrate mimic. The AMBER tLEAP module was used to add the missing residues and atoms.[2] The hydrogen atoms were added using the H++ program,[3] and SO_3 was mutated to dianionic or monoanionic phosphite (HPO_3^{2-} or $H_2PO_3^-$). For the monoanionic phosphite species, initially the hydrogen was located on the O_A oxygen, where it is pointed toward Gly77. After this substrate conversion, the substrate was optimized at the QM/MM level with only the substrate treated quantum mechanically and the rest of the system fixed. All QM/MM calculations were performed with the QM region treated at the DFT B3LYP/6-31G** level of theory,[4-6] and details about the MM force field are given below.

The QM region used in the finite temperature string simulations was determined by starting with a larger QM region that included Arg301 and decreasing its size while testing for convergence of the optimized geometry. In these tests, inclusion of Arg301 in the QM region did not significantly influence the optimized geometry, and therefore this residue was included in the MM region instead. Note that diffuse basis functions are advisable for anionic species but would significantly increase the computational expense of the finite temperature string calculations. The impact of diffuse basis functions was investigated by performing single-point energy calculations on QM configurations obtained from a series of different images associated with the reactant, top of the barrier, and product from the last iteration of a converged string. The relative energies of these configurations upon including diffuse basis functions was found to be less than ~3 kcal/mol and often less than ~1 kcal/mol. Thus, we do not expect the inclusion of diffuse basis functions to alter the qualitative conclusions of this work.

The putative general base, His292, was checked manually to ensure the protonation form of HID, which has a proton on the delta nitrogen, leaving the epsilon nitrogen free to act as the general base. The active site proximal water, HOH676, was manually moved closer to the phosphite and His292 to facilitate nucleophilic attack of the phosphite and proton transfer to His292. For the initial equilibration, this water was in the proximal position relative to the NAD^+ cofactor. The position of this water molecule was optimized at the QM/MM level with the water

molecule described quantum mechanically and the rest of the system was represented by the AMBER ff14SB force field[7] prior to solvation and equilibration.

Following this initial preparation, each of the two systems corresponding to the dianionic or monoanionic phosphite substrate was solvated with TIP3P waters, followed by neutralization of the system with Na^+ ions and addition of more Na^+ and Cl^- ions to achieve a concentration of ~0.15 M NaCl.[8] The AMBER ff14SB force field was used to describe the protein, and the parameters for NAD^+/NADH were obtained from a previous study.[9-10] The RESP procedure was performed to determine the partial atomic charges for the monoanionic and dianionic phosphite.[11-12] For this purpose, geometry optimizations were performed using Gaussian09,[13] followed by a two-stage RESP charge fitting based on the optimized geometry using the antechamber program in AmberTools.[2] The resulting charges are provided in Table S1 and Table S2. To maintain a stable monoanionic phosphite species during molecular dynamics, the van der Waals radius and well-depth of the hydroxyl proton were treated as 1.487 Å and 0.0157 kcal/mol in the 12-6 Lennard-Jones potential, respectively. The protocol for equilibration of the system using classical molecular dynamics was the same as that described previously.[14-15] For the equilibration, periodic boundary conditions were used, and the long-range electrostatics was described with the particle mesh Ewald (PME) method.[16] The time step for all molecular dynamics simulations was 1 fs.

After equilibration of the systems corresponding to the dianionic or monoanionic O_A phosphite substrates with the proximal attacking water position, we generated the other four systems studied. The monoanionic O_B system with proximal water was generated from the monoanionic O_A substrate system by moving the proton manually from O_A to O_B and optimizing its position at the QM/MM level, treating only the phosphite molecule quantum mechanically and keeping everything fixed except this molecule. The systems with the attacking water in the distal position were generated from each of these three systems with different substrates by moving the water manually and optimizing only this water molecule at the QM/MM level, treating only this water molecule quantum mechanically and keeping the remainder of the system fixed. The distal water was placed in a position that would enable an in-line geometry as well as deprotonation by His292, but upon geometry optimization, steric constraints from the protein (i.e., Arg237) resulted in geometries that were not as conducive to the in-line geometry characteristic of the associative mechanism.

After preparing these six systems in the reactant state, the corresponding product structures were generated. For each of the six systems, the hydride was manually moved to the NAD^+ C19 atom, producing NADH. In addition, the proton on the active site water was transferred to His292, and the hydroxide was moved to create the resulting phosphate species. Every atom manually moved was optimized at the QM/MM level of theory with the rest of the system fixed, followed by optimization of the entire QM region with the MM region fixed. Prior to the QM/MM simulations, the system was truncated to retain only the water molecules within 18 Å from any protein atom. During the QM/MM free energy simulations, only the residues with any atom within 18 Å of the phosphorus atom of the phosphite substrate were allowed to move.

We also constructed intermediate structures from the optimized reactant structures in a manner similar to the generation of the product structures. The trigonal planar dissociative mechanism intermediate was found through QM/MM geometry optimization, but this structure appeared to be highly strained. Multiple QM/MM geometry optimizations were attempted to search for the pentacoordinated associative mechanism intermediate, but no stable minimum was found. We initiated strings corresponding to the dissociative mechanism using a quadratic interpolation involving the reactant, intermediate, and product structures, but these strings were unstable, most likely because the intermediate states were high in energy. Similar attempts to initiate strings corresponding to the associative mechanism were not successful.

To further investigate the possibility of a pentacoordinated intermediate, additional QM/MM MD simulations were performed. These simulations started with a configuration obtained from an image corresponding to the top of the free energy barrier for the last iteration of either the monoO_A-distal or the monoO_B-distal converged string. Initially, the five bond lengths involving the central phosphorus were restrained to distances corresponding to the putative pentavalent intermediate using harmonic restraints with force constants of either 200 or 300 kcal/mol · $Å^{-2}$. The distances for the restraints on the P—H and P—OH bonds were obtained from the optimized transition state of a gas phase model system.[17] The distances for the restraints on the other three P—O bonds were obtained from the average distances sampled in the image corresponding to the top of the free energy barrier for the last iteration of either the monoO_A-distal or the monoO_B-distal converged string. After 100 fs of QM/MM MD with these bond lengths restrained, another 100 fs of QM/M MD without any restraints was performed. In the four independent trajectories propagated, the hydride transferred almost immediately upon releasing

the bond restraints (Table S8). These results indicate that the putative pentavalent intermediate is highly unstable.

All of the string simulations presented in the main paper were initiated from strings corresponding to a linear interpolation between the reactant and product structures described above. This initial string was divided into 30 images, and the value of each of the seven reaction coordinates for each image was used to define the harmonic restraints on the reaction coordinates for umbrella sampling. The force constants for the harmonic restraints were 100 kcal/mol·Å^{-2} and were increased to 150 kcal/mol to enhance the sampling of the transition state for iterations 5–10. The mobile MM region for every image was equilibrated for 10 ps while freezing the QM region. After the MM equilibration, each image was equilibrated with QM/MM molecular dynamics for 100 fs with the harmonic restraints on the reaction coordinates. After this initial equilibration for each image, the protocol for the finite temperature string method with umbrella sampling described elsewhere was followed.[15, 18-19] For each iteration, 100 fs of QM/MM molecular dynamics for each image was propagated with the umbrella sampling restraints based on the average values of the reaction coordinates from the previous iteration. After each iteration, the images were redistributed with even spacing along the string fitted based on the average values of the reaction coordinates for that iteration. This procedure was followed until the convergence criteria were satisfied. Specifically, the first convergence criterion is that the root-mean-square deviation (RMSD) value for all reaction coordinates relative to their average values from the previous five iterations is less than 0.1 Å (Figure S10). The second convergence criterion is that the free energy barrier changes by less than 0.5 kcal/mol between iterations (Figures S11). The changes in the free energy barrier and the reaction free energy between iterations 20 and 25 are given in Table S7 and further demonstrate that convergence is satisfied.

Table S1. Partial Atomic Charges Obtained using RESP for Dianionic Phosphite[a]

Atom Name	Atom Type	RESP Charge
P1	P5	1.386647
H1	HP	-0.358890
O1	O2	-1.009252
O2	O2	-1.009252
O3	O2	-1.009252

[a] To facilitate the analysis and discussion, O1 is denoted O_B, and O2 is denoted O_A in the main paper.

Table S2. Partial Atomic Charges Obtained using RESP for Monoanionic Phosphite[a]

Atom Name	Atom Type	RESP Charge
P1	P	1.286402
H1	HA	-0.208631
O1	O2	-0.859331
O2	O2	-0.859331
O3	OH	-0.742279
H3	HO	0.383171

[a] To facilitate the analysis and discussion, O1 is denoted O_B, and O2 is denoted O_A in the main paper.

Table S3. Important Active Site Hydrogen-Bonding Interactions with the Water in the Proximal Position[a]

	Dianionic-proximal			$MonoO_A$-proximal			$MonoO_B$-proximal		
	Distance	Angle	%	Distance	Angle	%	Distance	Angle	%
Arg237:N_1-PT:O_C[b]	2.8	161	89	2.8	161	84	2.9	158	93
Arg237:N_2-PT:O_C[b]	2.9	148	18	2.9	147	13	2.8	149	34
GLU266:$O_{E'}$-His292N_D	2.8	162	76	2.7	165	85	2.7	164	90
LYS76:N-PT:O_A	2.9	158	86	3.0	150	58	2.9	157	81
GLY77:N-PT:O_A	2.9	165	68	2.9	153	43	2.9	165	77
ASP79:O_{D1}-ARG237:N_E	2.8	152	56	2.8	151	61	2.7	150	61
ASP79:O_{D2}-ARG237:N_E	2.9	155	56	2.8	154	79	2.9	153	76

[a] All units are in Angstroms or Degrees. Columns for each species are in the order of average distance, average angle, and percentage of conformations in which the hydrogen bond was observed for the entire string simulation including all images for the final iteration. A hydrogen bond is determined based on the criteria that the donor-acceptor distance is less than or equal to 3.2 Å, and the angle of the donor, hydrogen, and acceptor is greater than or equal to 135°.
[b] This oxygen atom corresponds to the phosphite (PT) atom that is pointed toward the Arg237 residue.

Table S4. Important Active Site Hydrogen-Bonding Interactions with the Water in the Distal Position[a]

	Dianionic-distal			$MonoO_A$-distal			$MonoO_B$-distal		
	Distance	Angle	%	Distance	Angle	%	Distance	Angle	%
Arg237:N_1-PT:O_C[b]	2.8	165	79	2.9	161	82	2.8	163	83
Arg237:N_2-PT:O_C[b]	2.9	164	68	2.8	145	6	3.0	147	2
GLU266:$O_{E'}$-His292N_D	2.8	164	70	2.8	166	82	2.8	164	80
LYS76:N-PT:O_A	2.9	156	74	3.0	154	24	3.0	157	63
GLY77:N-PT:O_A	2.9	164	83	2.9	159	34	2.9	164	74
ASP79:O_{D1}-ARG237:N_E	2.7	152	47	2.8	150	69	2.7	150	64
ASP79:O_{D2}-ARG237:N_E	2.8	156	58	2.9	149	75	2.9	153	70

[a] All units are in Angstroms or Degrees. Columns for each species are in the order of average distance, average angle, and percentage of conformations in which the hydrogen bond was observed for the entire string simulation including all images for the final iteration. A hydrogen bond is determined based on the criteria that the donor-acceptor distance is less than or equal to 3.2 Å, and the angle of the donor, hydrogen, and acceptor is greater than or equal to 135°.
[b] This oxygen atom corresponds to the phosphite (PT) atom that is pointed toward the Arg237 residue.

Table S5: Important Active Site Hydrogen-Bonding Interactions with the Water in the Proximal Position for the Reactant and Product Configurations[a]

	Dianionic-proximal		$MonoO_A$-proximal		$MonoO_B$-proximal	
	R %	P %	R %	P %	R %	P %
Arg237:N_1-PT:O_C[b]	91	100	57	100	83	100
Arg237:N_2-PT:O_C[b]	27	70	0	17	21	0
GLU266:$O_{E'}$-His292:N_D	63	100	67	100	100	100
LYS76:N-PT:O_A	98	32	30	67	75	94
GLY77:N-PT:O_A	75	89	47	10	100	48
ASP79:O_{D1}-ARG237:N_E	61	32	49	96	87	82
ASP79:O_{D2}-ARG237:N_E	46	79	73	40	72	70

[a] A hydrogen bond is determined based on the criteria that the donor-acceptor distance is less than or equal to 3.2 Å, and the angle of the donor, hydrogen, and acceptor is greater than or equal to 135°. The percentage population of each hydrogen bond for the reactant and product configurations are given for these important hydrogen bonds. R and P correspond to the images associated with the reactant and product, respectively, along the MFEP.
[b] This oxygen atom corresponds to the phosphite (PT) atom that is pointed toward the Arg237 residue.

Table S6: Important Active Site Hydrogen-Bonding Interactions with the Water in the Distal Position for Reactant and Product Configurations[a]

	Dianionic-distal		$MonoO_A$-distal			$MonoO_B$-distal		
	R %	P %	R %	I %	P %	R %	I %	P %
Arg237:N_1-PT:O_C[b]	100	100	71	41	98	95	51	96
Arg237:N_2-PT:O_C[b]	14	0	22	0	19	0	0	0
GLU266:$O_{E'}$-His292:N_D	63	75	100	75	100	42	84	100
LYS76:N-PT:O_A	85	19	0	91	0	79	64	23
GLY77:N-PT:O_A	100	72	0	99	15	87	79	100
ASP79:O_{D1}-ARG237:N_E	33	14	66	75	74	67	44	65
ASP79:O_{D2}-ARG237:N_E	55	75	60	89	64	77	99	78

[a] A hydrogen bond is determined based on the criteria that the donor-acceptor distance is less than or equal to 3.2 Å, and the angle of the donor, hydrogen, and acceptor is greater than or equal to 135°. The percentage population of each hydrogen bond for the reactant, intermediate, and product configurations are given for these important hydrogen bonds. R, I, and P correspond to the images associated with the reactant, intermediate, and product, respectively, along the MFEP.
[b] This oxygen atom corresponds to the phosphite (PT) atom that is pointed toward the Arg237 residue

Table S7: Change in Calculated Free Energy Barriers and Reaction Free Energies Between Iterations 20 and 25[a]

	Dianionic–proximal	$MonoO_A$–proximal	$MonoO_B$–proximal	Dianionic–distal	$MonoO_A$–distal[b]	$MonoO_B$–distal[b]
Free energy barrier	-1.6	-1.6	0.9	-1.8	0.6	-0.2
Reaction free energy	-1.0	-1.4	0.7	-1.4	-2.8	-1.4

[a] All units are in values of kcal/mol. $MonoO_A$ ($MonoO_B$) refers to the protonation of O_A (O_B) of the phosphite substrate.
[b] The free energy barrier is computed as the difference between the second barrier and the initial reactant, and the reaction free energy is computed as the difference between the final product and initial reactant free energies.

Table S8 QM/MM MD Simulations to Probe the Putative Pentacoordinated Intermediate [a]

	Initial distances	Distances after 100 fs restrained MD	Distances after 20 fs unrestrained MD	Distances after 50 fs unrestrained MD	Distances after 100 fs unrestrained MD
$P\text{-}O_{Nuc}$[b]	1.84	1.72	1.68	1.70	1.69
$P\text{-}O_C$[c]	1.55	1.52	1.54	1.55	1.48
$P\text{-}O_A$[c]	1.61	1.60	1.64	1.68	1.74
$P\text{-}O_B$[c]	1.52	1.50	1.54	1.51	1.55
P-H[b]	1.59	1.98	2.47	3.46	4.70
$P\text{-}O_{Nuc}$[b]	1.84	1.70	1.61	1.71	1.69
$P\text{-}O_C$[c]	1.55	154	1.61	1.56	1.48
$P\text{-}O_A$[c]	1.61	1.68	1.59	1.69	1.69
$P\text{-}O_B$[c]	1.52	1.50	1.52	1.53	1.47
P-H[b]	1.59	1.78	2.39	3.46	4.32
$P\text{-}O_{Nuc}$[b]	1.84	1.72	1.64	1.70	1.64
$P\text{-}O_C$[d]	1.56	1.58	1.54	1.56	1.52
$P\text{-}O_A$[d]	1.54	1.53	1.56	1.53	1.52
$P\text{-}O_B$[d]	1.61	1.61	1.68	1.67	1.69
P-H[b]	1.59	1.99	2.30	2.82	4.09
$P\text{-}O_{Nuc}$[b]	1.84	1.79	1.61	1.62	1.58
$P\text{-}O_C$[d]	1.56	1.56	1.54	1.56	1.51
$P\text{-}O_A$[d]	1.54	1.55	1.57	1.57	1.51
$P\text{-}O_B$[d]	1.61	1.64	1.64	1.65	1.64
P-H[b]	1.59	1.56	2.23	2.76	3.78

[a] All distances are given in Angstroms. For the restrained MD, the distances are restrained to the initial values given in the table with harmonic force constants of 200 kcal/mol·$Å^{-2}$ (first set of data given for each set of initial distances) or 300 kcal/mol·$Å^{-2}$ (second set of data given for each set of initial distances).
[b] Values obtained from the transition state computed for a gas phase model system.[17]
[c] Values obtained from the average distances sampled in the image corresponding to the top of the barrier in the last iteration of the $monoO_A$-distal string.
[d] Values obtained from the average distances sampled in the image corresponding to the top of the barrier in the last iteration of the $monoO_B$-distal string.

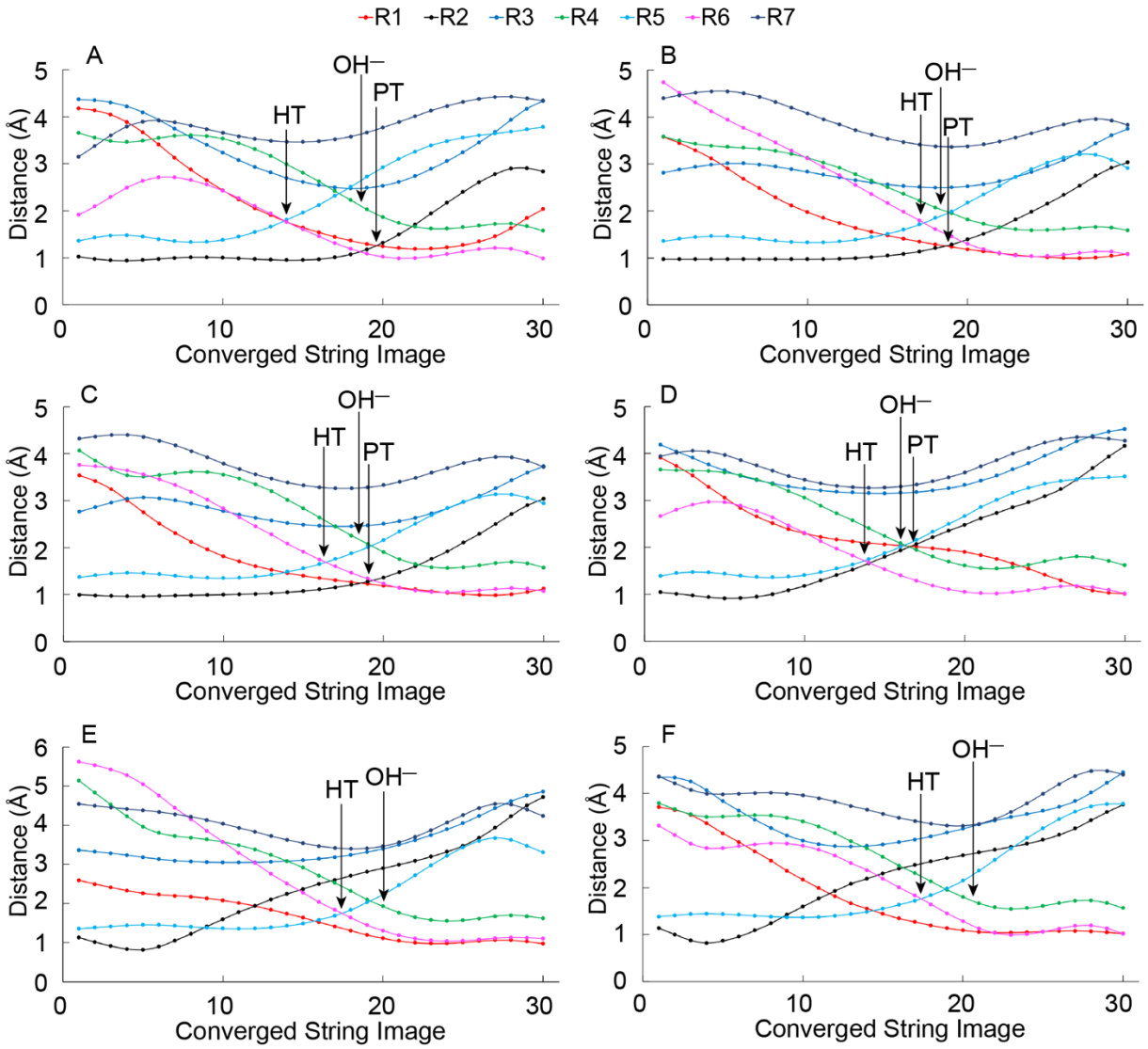

Figure S1: The values of all seven reaction coordinates along the MFEP as a function of the string image for the converged (A) dianionic-proximal, (B) monoO$_A$-proximal, (C) monoO$_B$-proximal, (D) dianionic-distal, (E) monoO$_A$-distal, and (F) monoO$_B$-distal strings. The seven reaction coordinates are defined in Figure 3. Hydride transfer is indicated by the crossing of R5 and R6, nucleophilic water attack is indicated by R4 becoming ~1.6 Å, and proton transfer from water to His292 is indicated by the crossing of R1 and R2. Note that in E and F the proton transfer that occurs early in the mechanism is part of the pre-equilibrium process discussed in the main text and is not part of the hydrolysis step that occurs concurrently with nucleophilic water attack later in the mechanism.

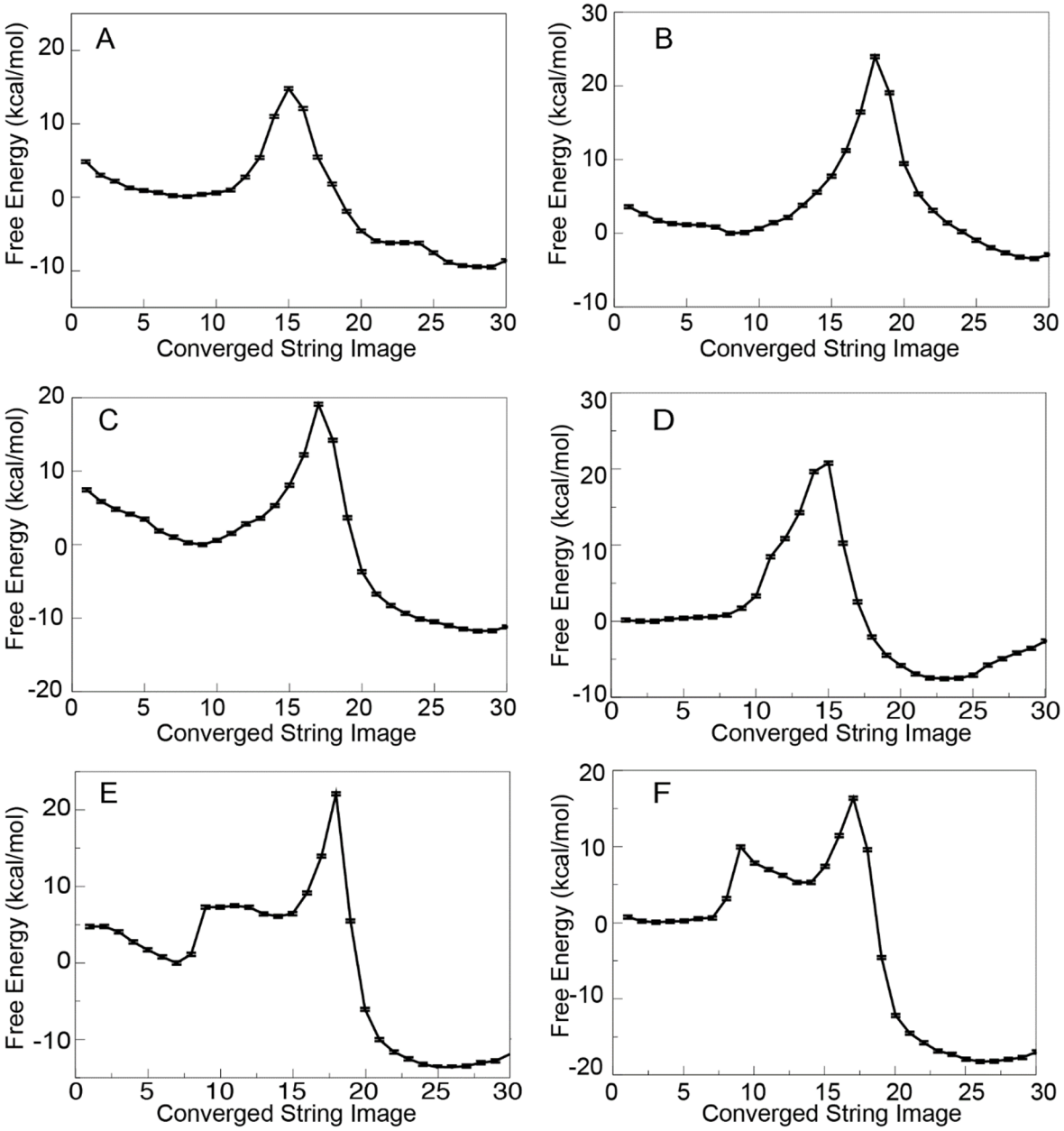

Figure S2: The free energy along the MFEP for the (A) dianionic-proximal, (B) monoO$_A$-proximal, (C) monoO$_B$-proximal, (D) dianionic-distal, (E) monoO$_A$-distal, and (F) monoO$_B$-distal strings. The error bars in the free energy profiles along the MFEP correspond to the statistical errors of the WHAM procedure and were obtained using a bootstrapping error analysis with 20 "fake" data sets. Note that these error bars do not account for errors arising from the level of theory used to generate the potential energy surface and the limited conformational sampling.

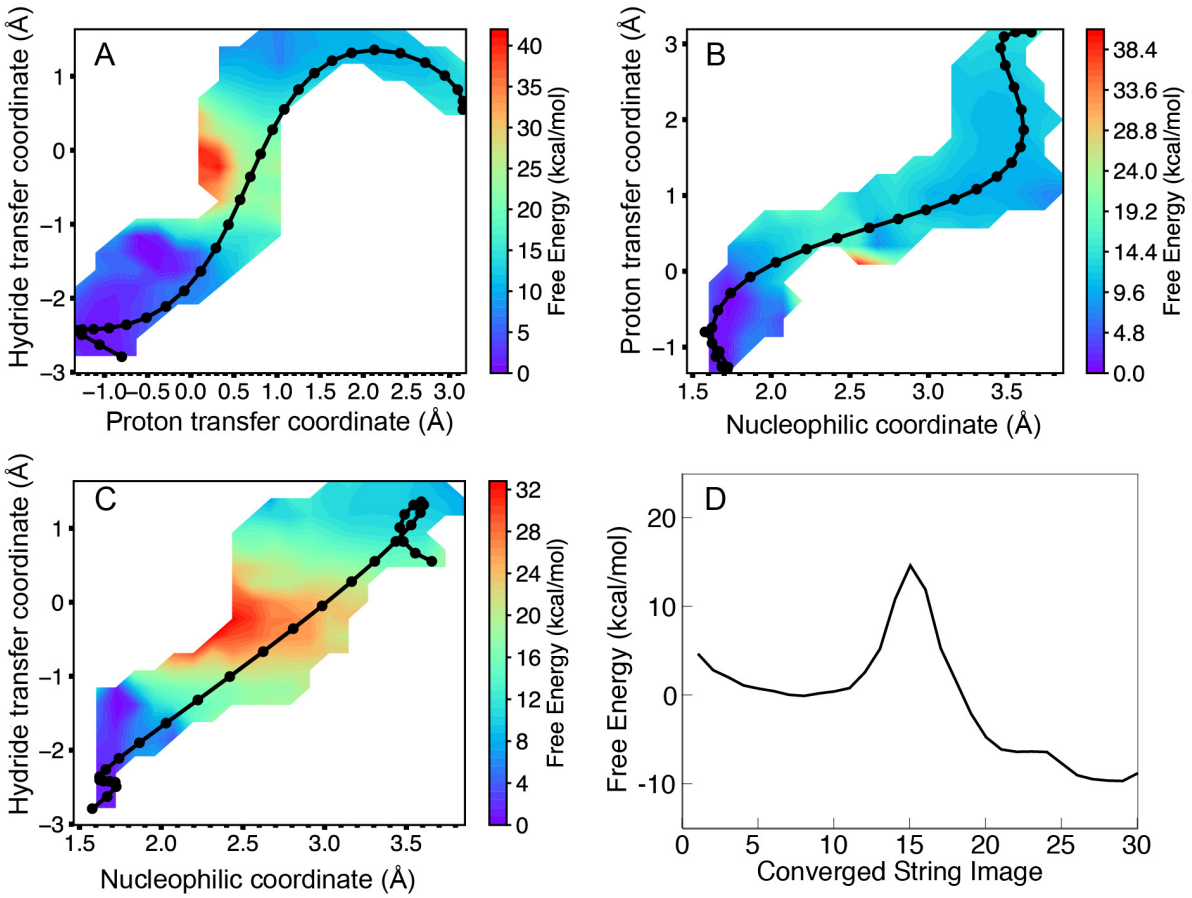

Figure S3: Two dimensional free energy surfaces and the converged string in black for the dianionic phosphite substrate with the attacking water in the proximal position projected onto the reaction coordinates corresponding to (A) proton transfer from water to His292 and hydride transfer, (B) nucleophilic water attack and proton transfer from water to His292; and (C) nucleophilic water attack and hydride transfer. The free energy along the MFEP as a function of the string image is given in (D).

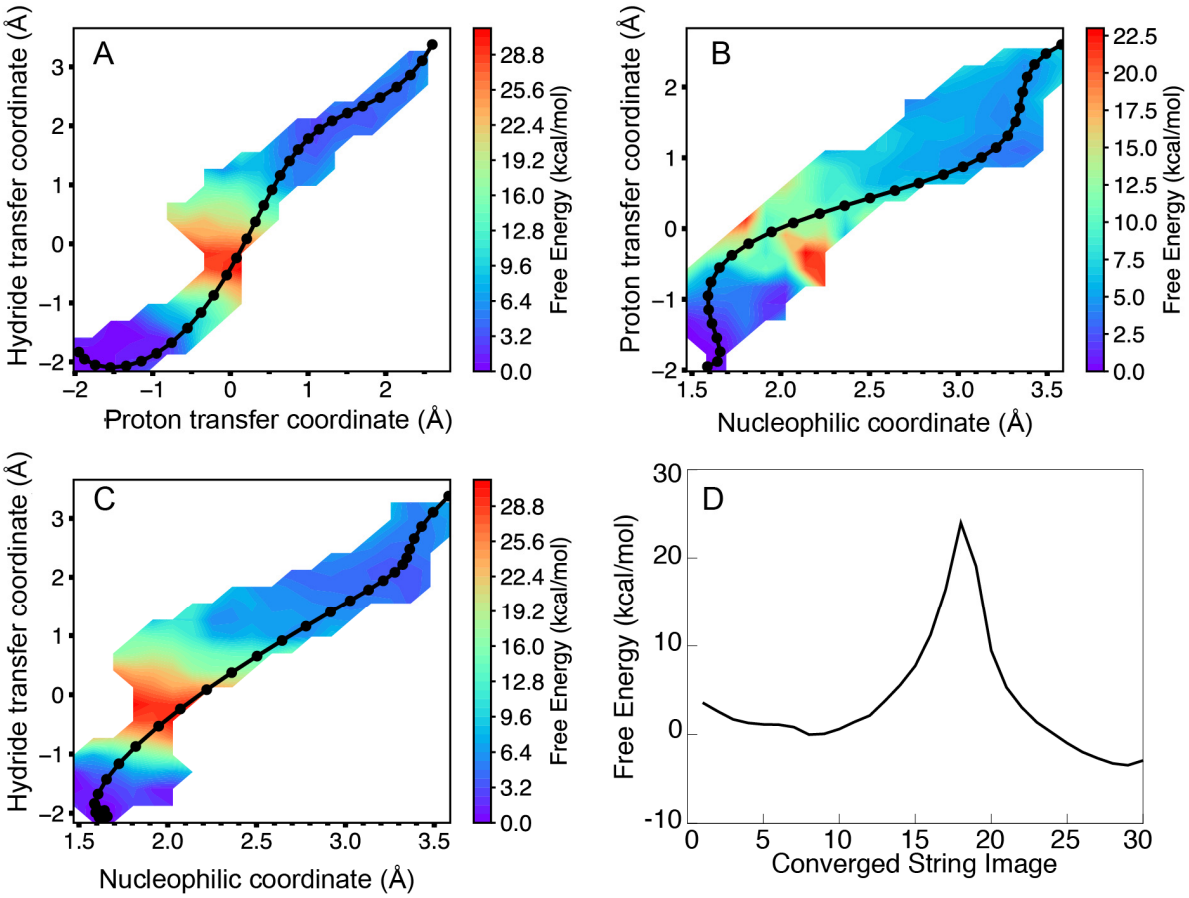

Figure S4: Two dimensional free energy surfaces and the converged string in black for the monoanionic phosphite substrate with O_A protonated and the attacking water in the proximal position projected onto the reaction coordinates corresponding to (A) proton transfer from water to His292 and hydride transfer, (B) nucleophilic water attack and proton transfer from water to His292; and (C) nucleophilic water attack and hydride transfer. The free energy along the MFEP as a function of the string image is given in (D).

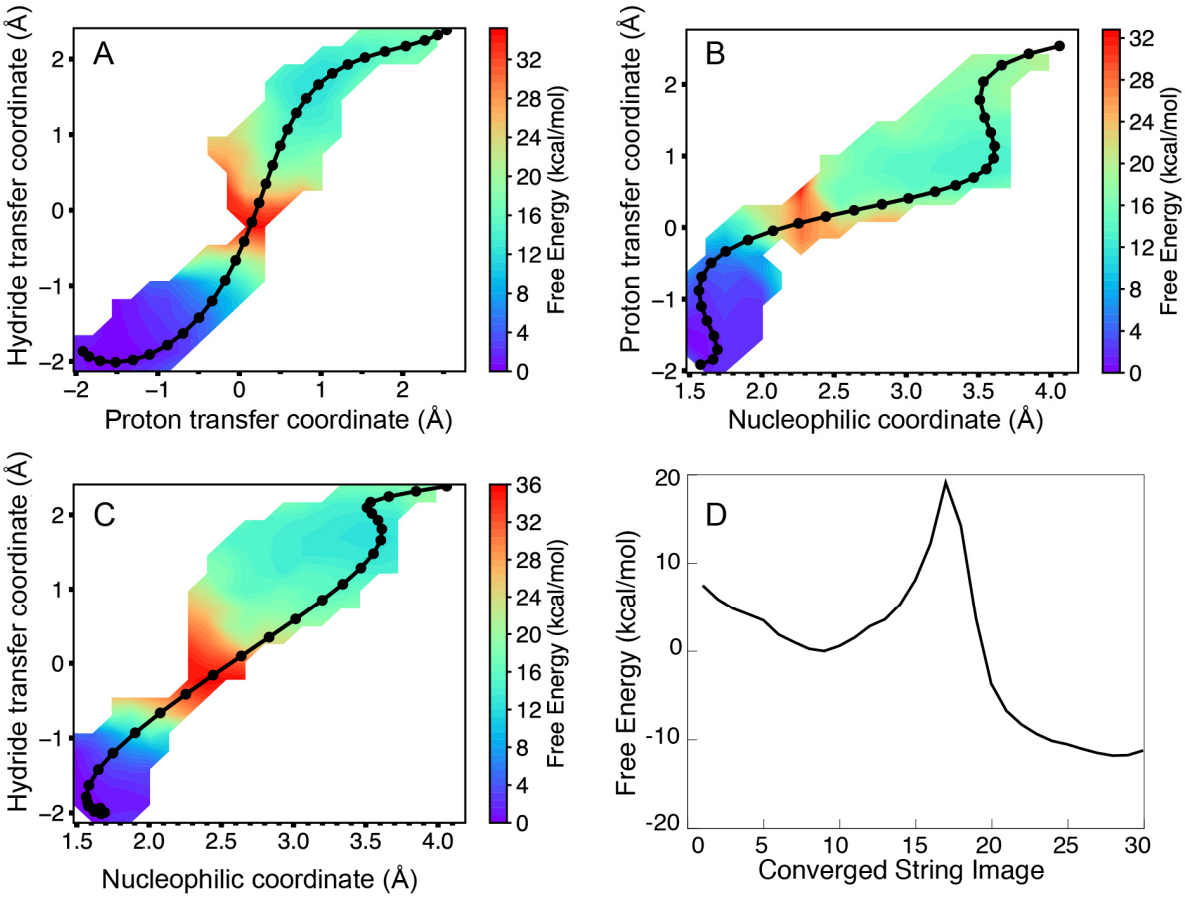

Figure S5: Two dimensional free energy surfaces and the converged string in black for the monoanionic phosphite substrate with O_B protonated and the attacking water in the proximal position projected onto the reaction coordinates corresponding to (A) proton transfer from water to His292 and hydride transfer, (B) nucleophilic water attack and proton transfer from water to His292; and (C) nucleophilic water attack and hydride transfer. The free energy along the MFEP as a function of the string image is given in (D).

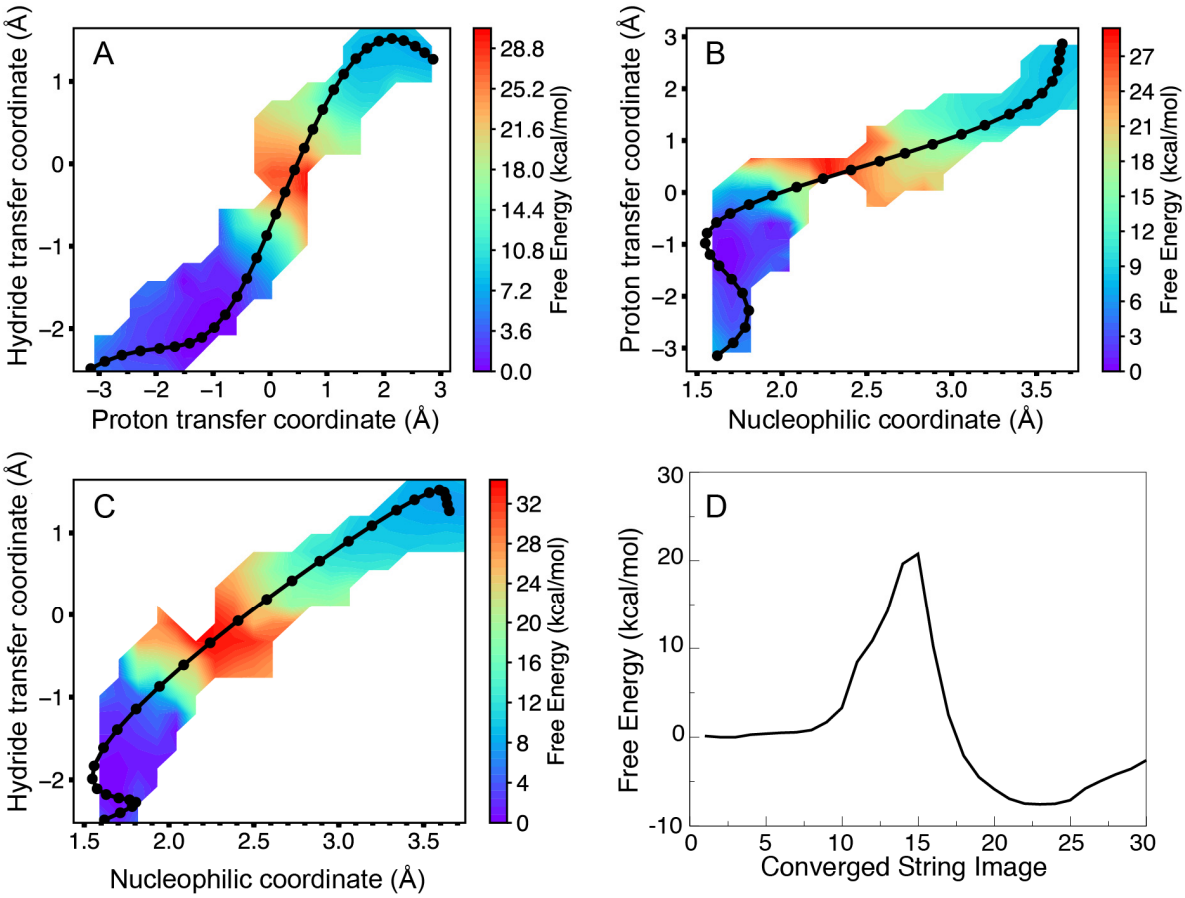

Figure S6: Two dimensional free energy surfaces and the converged string in black for the dianionic phosphite substrate and the attacking water in the distal position projected onto the reaction coordinates corresponding to (A) proton transfer from water to His292 and hydride transfer, (B) nucleophilic water attack and proton transfer from water to His292; and (C) nucleophilic water attack and hydride transfer. The free energy along the MFEP as a function of the string image is given in (D).

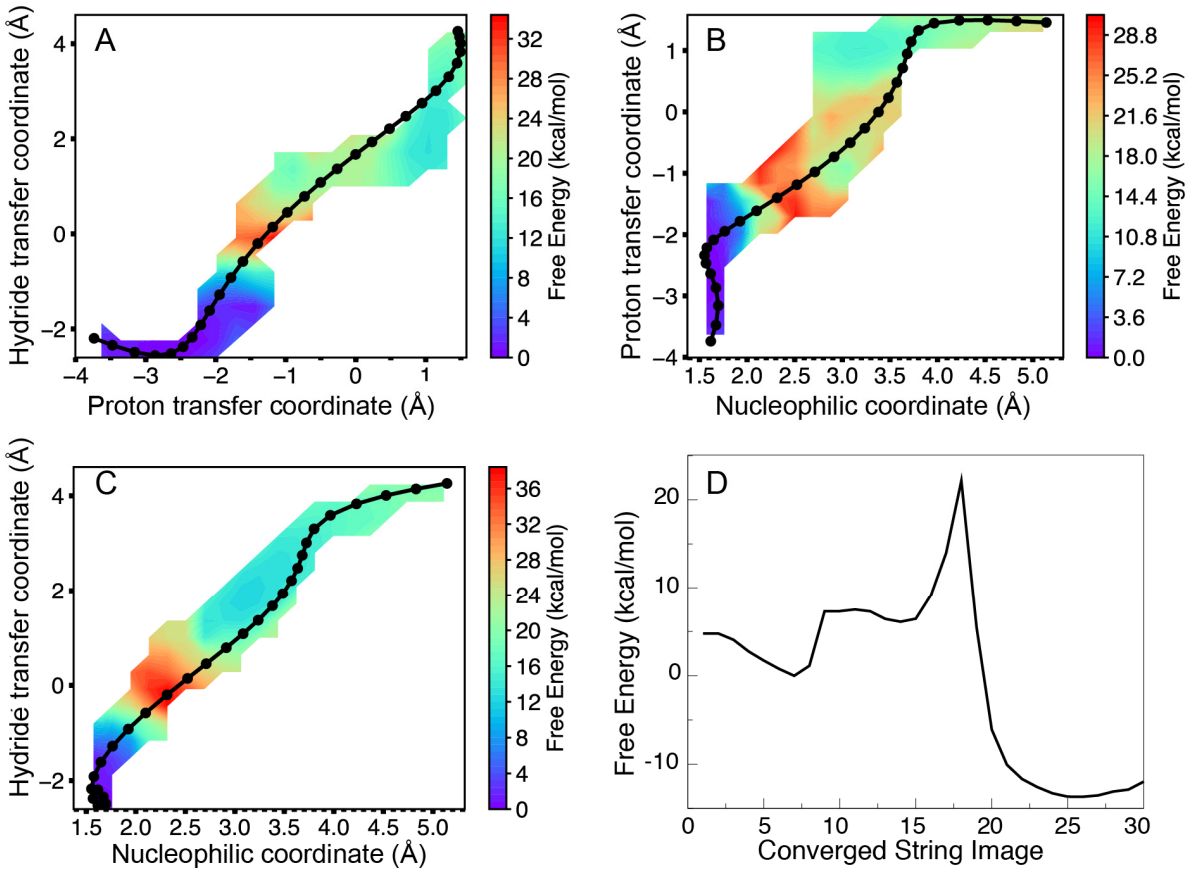

Figure S7: Two dimensional free energy surfaces and the converged string in black for the monoanionic phosphite substrate with O_A protonated and the attacking water in the distal position projected onto the reaction coordinates corresponding to (A) proton transfer from water to His292 and hydride transfer, (B) nucleophilic water attack and proton transfer from water to His292; and (C) nucleophilic water attack and hydride transfer. The free energy along the MFEP as a function of the string image is given in (D). For this string, the proton transfer occurs early in the mechanism and is part of the pre-equilibrium process discussed in the main text. This proton transfer is not part of the hydrolysis step that occurs concurrently with nucleophilic water attack later in the mechanism.

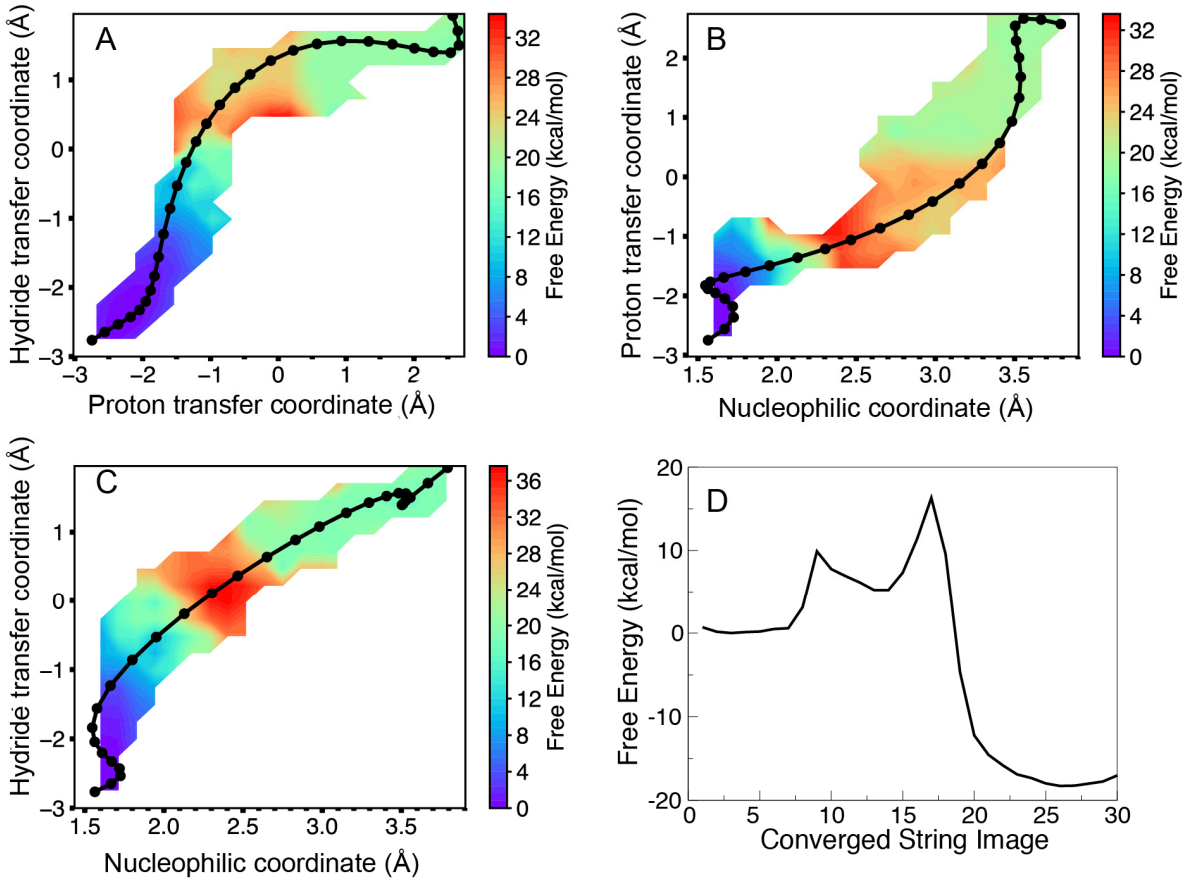

Figure S8: Two dimensional free energy surfaces and the converged string in black for the monoanionic phosphite substrate with O_B protonated and the attacking water in the distal position projected onto the reaction coordinates corresponding to (A) proton transfer from water to His292 and hydride transfer, (B) nucleophilic water attack and proton transfer from water to His292; and (C) nucleophilic water attack and hydride transfer. The free energy along the MFEP as a function of the string image is given in (D). For this string, the proton transfer occurs early in the mechanism and is part of the pre-equilibrium process discussed in the main text. This proton transfer is not part of the hydrolysis step that occurs concurrently with nucleophilic water attack later in the mechanism.

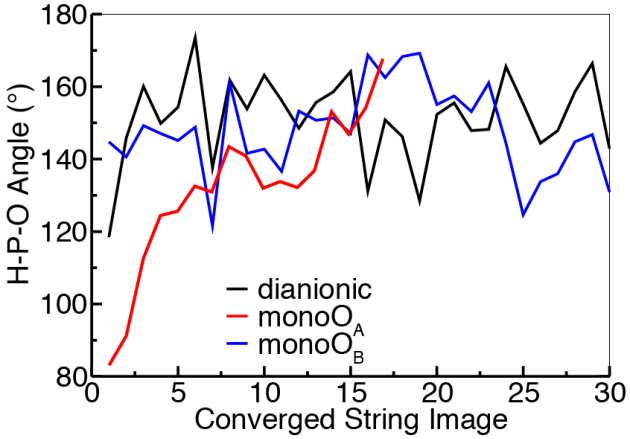

Figure S9: Average angle between the nucleophilic water oxygen, the phosphorus, and the transferring hydride for each image of the last iteration of the converged distal strings. The dianionic-distal, monoO$_A$-distal, and monoO$_B$-distal strings are represented in black, red, and blue, respectively. The average angles during the nucleophilic attack (i.e., averaged over the images spanning the relevant barrier for each string) are 148, 157, and 167 for the dianionic-distal, monoO$_A$-distal, and monoO$_B$-distal strings, respectively, suggestive of a nearly in-line geometry. The red line is terminated at the point where the product rotates in a manner that scrambles the oxygen atoms, thereby altering the definition of this angle.

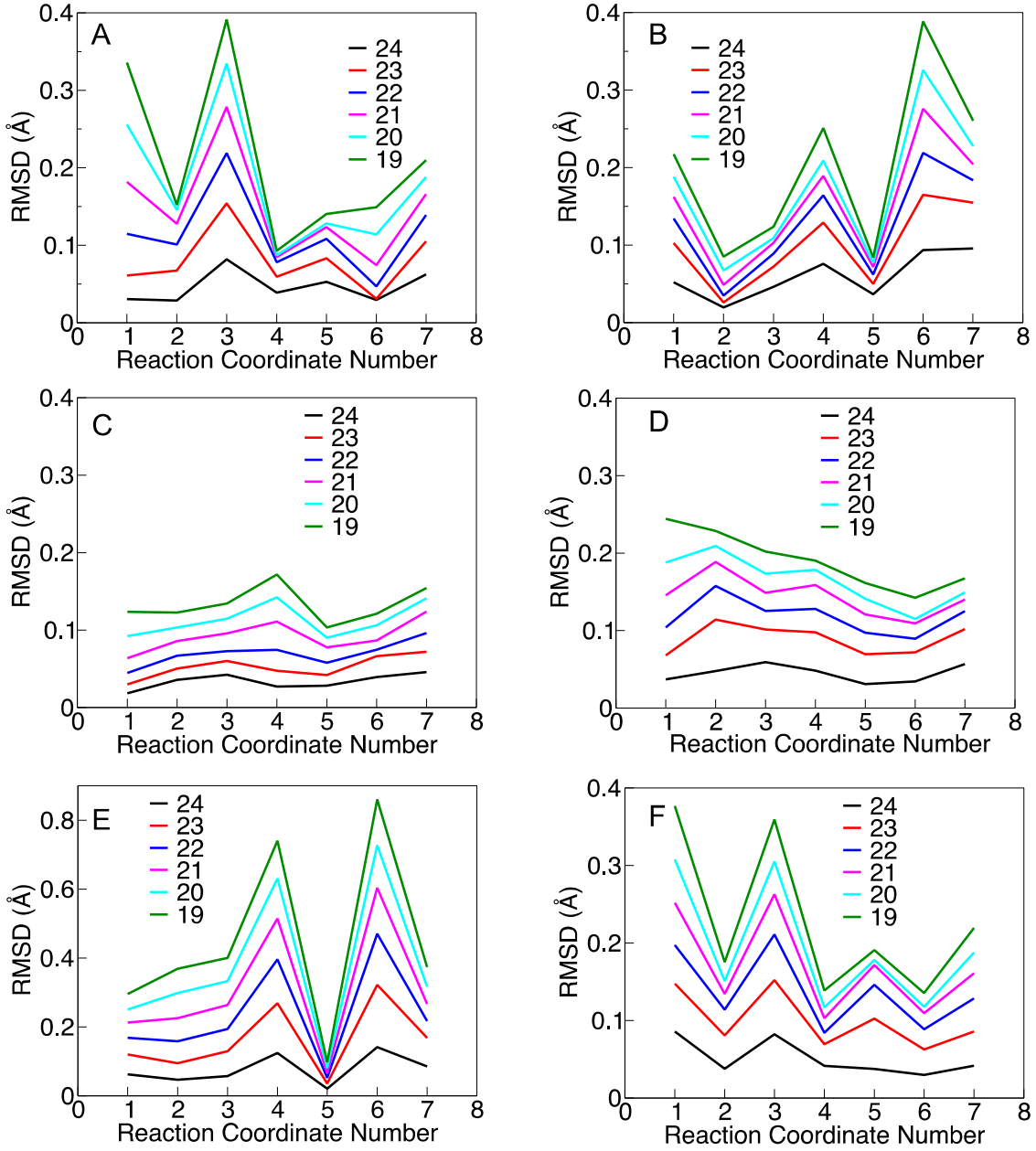

Figure S10: The root-mean-square deviation (RMSD) of each reaction coordinate for the iterations indicated in the legend. The RMSD of each reaction coordinate for the specified iteration was calculated relative to its value averaged over the previous five iterations for the (A) dianionic-proximal, (B) monoO$_A$-proximal, (C) monoO$_B$-proximal, (D) dianionic-distal, (E) monoO$_A$-distal, and (F) monoO$_B$-distal strings. This figure indicates that the RMSD for all reaction coordinates of all six strings is below 0.1 Å for the final iteration.

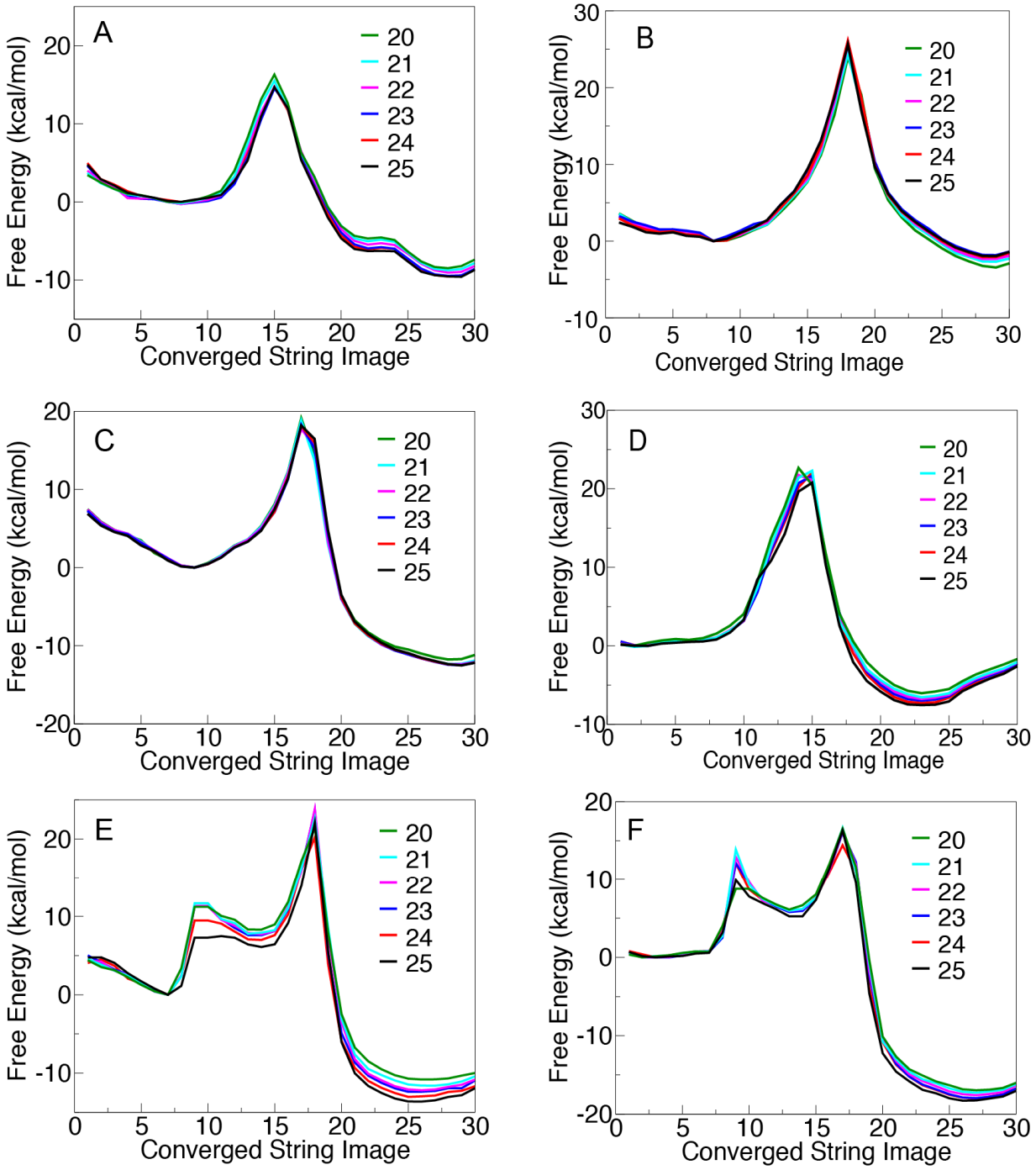

Figure S11: Free energy profiles along the MFEPs for the last five iterations, illustrating convergence of the mechanism and the relative free energies for the (A) dianionic-proximal, (B) monoO$_A$-proximal, (C) monoO$_B$-proximal, (D) dianionic-distal, (E) monoO$_A$-distal, and (F) monoO$_B$-distal strings. This figure indicates that the free energy barrier is changing by less than 0.5 kcal/mol between these iterations.

References

1. Zou, Y. Z.; Zhang, H. J.; Brunzelle, J. S.; Johannes, T. W.; Woodyer, R.; Hung, J. E.; Nair, N.; van der Donk, W. A.; Zhao, H. M.; Nair, S. K., Crystal Structures of Phosphite Dehydrogenase Provide Insights into Nicotinamide Cofactor Regeneration. *Biochemistry* **2012,** *51*, 4263-4270.
2. D.A. Case, V. B., J.T. Berryman, R.M. Betz, Q. Cai, D.S. Cerutti, T.E. Cheatham, III, T.A. Darden, R.E. Duke, H. Gohlke, A.W. Goetz, S. Gusarov, N. Homeyer, P. Janowski, J. Kaus, I. Kolossváry, A. Kovalenko, T.S. Lee, S. LeGrand, T. Luchko, R. Luo, B. Madej, K.M. Merz, F. Paesani, D.R. Roe, A. Roitberg, C. Sagui, R. Salomon-Ferrer, G. Seabra, C.L. Simmerling, W. Smith, J. Swails, R.C. Walker, J. Wang, R.M. Wolf, X. Wu and P.A. Kollman *AMBER 14*, University of California, San Francisco.: 2014.
3. Gordon, J. C.; Myers, J. B.; Folta, T.; Shoja, V.; Heath, L. S.; Onufriev, A., H++: a server for estimating pK(a)s and adding missing hydrogens to macromolecules. *Nucleic Acids Res.* **2005,** *33*, W368-W371.
4. Hehre, W. J.; Lathan, W. A., Self-Consistent Molecular-Orbital Methods .XIV. Extended Gaussian-Type Bases for Molecular-Orbital Studies of Organic-Molecules - Inclusion of Second Row Elements. *J. Chem. Phys.* **1972,** *56*, 5255-5257.
5. Lee, C.; Yang, W.; Parr, R. G., Development of the Colle-Salvetti correlation-energy formula into a functional of the electron density. *Phys. Rev. B* **1988,** *37*, 785-789.
6. Becke, A. D., Density-functional thermochemistry. III. The role of exact exchange. *J. Chem. Phys.* **1993,** *98*, 5648-5652.
7. Maier, J. A.; Martinez, C.; Kasavajhala, K.; Wickstrom, L.; Hauser, K. E.; Simmerling, C., ff14SB: Improving the Accuracy of Protein Side Chain and Backbone Parameters from ff99SB. *J. Chem. Theory Comput.* **2015,** *11*, 3696-3713.
8. Jorgensen, W. L.; Chandrasekhar, J.; Madura, J. D.; Impey, R. W.; Klein, M. L., Comparison of Simple Potential Functions for Simulating Liquid Water. *J. Chem. Phys.* **1983,** *79*, 926-935.
9. Ryde, U., On the role of Glu-68 in alcohol dehydrogenase. *Protein Sci.* **1995,** *4*, 1124-32.
10. Ryde, U., Molecular-Dynamics Simulations of Alcohol-Dehydrogenase with a 4-Coordinate or 5-Coordinate Catalytic Zinc Ion. *Proteins* **1995,** *21*, 40-56.
11. Cornell, W. D.; Cieplak, P.; Bayly, C. I.; Kollman, P. A., Application of RESP Charges to Calculate Conformational Energies, Hydrogen-Bond Energies, and Free-Energies of Solvation. *J. Am. Chem. Soc.* **1993,** *115*, 9620-9631.
12. Cieplak, P.; Cornell, W. D.; Bayly, C.; Kollman, P. A., Application of the Multimolecule and Multiconformational Resp Methodology to Biopolymers - Charge Derivation for DNA, Rna, and Proteins. *J. Comput. Chem.* **1995,** *16*, 1357-1377.
13. Frisch, M. J. T., G. W.; Schlegel, H. B.; Scuseria, G. E.;; Robb, M. A. C., J. R.; Scalmani, G.; Barone, V.; Mennucci, B.;; Petersson, G. A. N., H.; Caricato, M.; Li, X.; Hratchian, H. P.;; Izmaylov, A. F. B., J.; Zheng, G.; Sonnenberg, J. L.; Hada, M.;; Ehara, M. T., K.; Fukuda, R.; Hasegawa, J.; Ishida, M.; Nakajima,; T.; Honda, Y. K., O.; Nakai, H.; Vreven, T.; Montgomery, J. A., Jr.;; Peralta, J. E. O., F.; Bearpark, M.; Heyd, J. J.; Brothers, E.; Kudin,; K. N.; Staroverov, V. N. K., T.; Kobayashi, R.; Normand, J.;; Raghavachari, K. R., A.; Burant, J. C.; Iyengar, S. S.; Tomasi, J.;; Cossi, M. R., N.; Millam, J. M.; Klene, M.; Knox, J. E.; Cross, J. B.;; Bakken, V. A., C.; Jaramillo, J.; Gomperts, R.; Stratmann, R. E.;; Yazyev, O. A., A. J.; Cammi, R.; Pomelli, C.; Ochterski, J. W.;; Martin, R. L. M., K.; Zakrzewski, V. G.; Voth, G. A.; Salvador,; P.; Dannenberg,

J. J. D., S.; Daniels, A. D.; Farkas, O.;; Foresman, J. B. O., J. V.; Cioslowski, J.; Fox, D. J. *Gaussian 09*, Gaussian Inc.: Wallingford, CT, 2009.
14. Ucisik, M. N.; Bevilacqua, P. C.; Hammes-Schiffer, S., Molecular Dynamics Study of Twister Ribozyme: Role of Mg^{2+} Ions and the Hydrogen-Bonding Network in the Active Site. *Biochemistry* **2016,** *55*, 3834-3846.
15. Stevens, D. R.; Hammes-Schiffer, S., Exploring the Role of the Third Active Site Metal Ion in DNA Polymerase eta with QM/MM Free Energy Simulations. *J. Am. Chem. Soc.* **2018,** *140*, 8965-8969.
16. Darden, T.; York, D.; Pedersen, L., Particle Mesh Ewald - an N.Log(N) Method for Ewald Sums in Large Systems. *J. Chem. Phys.* **1993,** *98*, 10089-10092.
17. Howe, G. W.; van der Donk, W. A., O-18 Kinetic Isotope Effects Reveal an Associative Transition State for Phosphite Dehydrogenase Catalyzed Phosphoryl Transfer. *J. Am. Chem. Soc.* **2018,** *140*, 17820-17824.
18. Ganguly, A.; Thaplyal, P.; Rosta, E.; Bevilacqua, P. C.; Hammes-Schiffer, S., Quantum mechanical/molecular mechanical free energy simulations of the self-cleavage reaction in the hepatitis delta virus ribozyme. *J. Am. Chem. Soc.* **2014,** *136*, 1483-1496.
19. Zhang, S.; Ganguly, A.; Goyal, P.; Bingaman, J. L.; Bevilacqua, P. C.; Hammes-Schiffer, S., Role of the active site guanine in the glmS ribozyme self-cleavage mechanism: Quantum mechanical/molecular mechanical free energy simulations. *J. Am. Chem. Soc.* **2015,** *137*, 784-798.